Assessment of the Correlation between Extreme Weather Event-Induced Human Mobility Perturbation in Urban Areas and their Spatial Characteristics based on Taxi Trajectories

Xinyuan Zhang
Department of Construction Management, Tsinghua University
xinyuan-16@mails.tsinghua.edu.cn

Nan Li
Department of Construction Management, Tsinghua University
nanli@tsinghua.edu.cn

ABSTRACT

Extreme weather events (EWEs) are significant threats to urban regions. One major reflection of such impact is the EWE-induced perturbation to urban human mobility, which has been documented in a number of recent studies. This study aims to examine the spatial distribution of such perturbation within a city among different areas that are characterized by the type of function and the distance to city center. A case study was conducted on a major rainstorm in the City of Nanjing, China in 2017, based on trajectories of all taxis in the city before and during the rainstorm. It was found that the rainstorm caused decrease in people's travel demand throughout the city, although the magnitude of perturbation and level of mobility resilience notably differed among areas of different functional types. In addition, the urban mobility in areas distant from the city center were relatively less influenced by rainstorm.

Keywords

Extreme weather event; Human mobility; Perturbation; Resilience; Spatial distribution

INTRODUCTION

Extreme weather events (EWEs), which are defined as events rarer than the 10^{th} or 90^{th} percentile of a probability density function estimated from observations at a certain place (IPCC, 2014), have been proved to increase in both frequency and intensity due to climate changes (Sobel and Tippett, 2018; Stott, 2016; Van Aalst, 2006). In the past few decades, EWEs have shown increasingly powerful influence to human beings and their habitats around the world. For example, in 2018, the top three most expensive EWEs in the United States, namely, hurricanes Florence and Michael as well as California's wildfires caused a total damage of over $41 billion (CBS NEWS, 2018). Moreover, recent research has projected that this trend will continue to expand in the future (Forzieri et al., 2016). Thus, there is increasing awareness across business, governments and civil society of the urgency of tackling risks from EWEs (Collins, 2018). This is of particular relevance to urban regions which, with large population and intensive assets, are extremely vulnerable to threats from EWEs (Force, 2013; Godschalk, 2003).

In recent years, with the increasing accessibility to various human mobility data through GPS, social media platforms and mobile phones, urban mobility provides a new perspective for assessing the impacts of EWEs. Perturbation to urban mobility can reflect the overall adverse influence of EWEs associated with reduced transportation infrastructure capacities, adverse weather and commuting conditions, interrupted economic activities and disturbed social dynamics (Zhang, 2019). An increasing volume of recent research has found that the statistical properties of human mobility at the population level, described by metrics such as travel displacement and radius of gyration, would be notably perturbed. For example, Wang and Taylor (2014) found

that the number of long-distance trips decreased while the number of short-distance trips increased during hurricane Sandy. The same phenomenon was also observed in another study that examined several severe winter storms in the northeastern United States (Wang et al., 2017). Yabe et al. (2016) found that the average movement of individuals showed an immediate increase in the aftermath of the Kumamoto Earthquake and then began to decrease after about an hour. Furthermore, the distribution of radius of gyration of the population may also change during abnormal time (Lu et al., 2016; Wang et al., 2017), and the average radius of gyration became much higher immediately after Haiti earthquake.

Meanwhile, despite the deviation of human mobility distribution, the overall mobility pattern has found to be resilient to some extent. For instance, Wang and Taylor (2014) found that human mobility possessed an inherent resilience even in abnormal time in a case study of Hurricane Sandy, suggesting the possibility of predicting mobility during hurricanes based on normal mobility data. Similar conclusion was also drawn in a study that investigated multiple types of natural disaster. The distribution of travel distance in abnormal time would still follow a power-law distribution and show significant correlation with that in normal time (Wang and Taylor, 2016). Existing studies have also developed a few metrics to quantify human mobility perturbation and resilience. For instance, Wang and Taylor (2016) used the shifting distance of center of mass between steady state and perturbation state to quantify the variation of individual mobility pattern. Zhang et al. (2019) proposed a new metric, termed relative total distance (RTD), to measure the instantaneous urban human mobility perturbation, and another metric, termed accumulated perturbation (AP) to measure the accumulated perturbation of human mobility in a city or its subareas.

Despite these prior studies, however, there is still limited understanding of urban human mobility perturbation during EWEs (Wang and Taylor, 2014). While most prior research focused on the overall human mobility perturbation in a city, there is a gap where the spatial distribution of human mobility perturbation, including the variance of perturbation among different areas in a city, has barely been examined. In the study of Zhang et al. (2019), a preliminary exploration of the spatial distribution of human mobility perturbation was conducted. It was found that the resilience of different areas in a city to the EWE impact, measured by the mobility perturbation, was significantly different. While such variance may be attributed to a range of factors, such as infrastructure service, local demographics and zone functionalities, the spatial characteristics of an urban area has been proven a major factor that is influential on people's commuting behavior (Beecham el al., 2014) hence on their mobility patterns. Exploring the relationship between the spatial characteristics of an urban area and the mobility perturbation of population located within the area may contribute to further understanding of the factors affecting urban resilience, thus helping answer questions such as what specific impacts different areas in cities would endure during EWEs, how to develop efficient measures to predict and mitigate possible EWE-induced impacts, and ultimately how to enhance the overall resilience of urban population when influenced by the EWEs.

Motivated by the above gap, this study aims to examine the spatial distribution of the impacts of EWEs on urban human mobility, and analyze the variance of mobility perturbation among urban areas with diverse spatial characteristics. Using the aforementioned two metrics (RTD and AP) developed by Zhang et al. (2019), this study examines the relationship between the EWE-induced human mobility perturbation in an urban area and the spatial characteristics of the area. The spatial characteristics of an urban area are describe based on its type of function that can be represented by points of interest (POIs) within the area, and its geolocation that is described based on its distance to the city center. Using taxi trajectory data, a case study was conducted in the City of Nanjing, the capital of Jiangsu Province in China. The case study focused on a major rainstorm event in June 2017, which severely impacted human mobility in the city.

Understanding and predicting human mobility in urban area has great importance to urban planning (Horner & O'Kelly, 2001), traffic prediction (Krings et al., 2009) as well as epidemics (Belik et al., 2011). Understanding human mobility under EWEs, in particular, would play a critical role in disaster response and risk reduction. Because without a deeper understanding of human mobility under EWEs, overcrowding in certain areas or overloading of infrastructure may affect the normal functions of cities. This study contributes to the existing body of knowledge by connecting the analysis of EWE-induced mobility perturbation with spatial characteristics of different areas in a city, which could shed new light on how and why human mobility perturbation varies within a city, and inform the development of appropriate area-specific measures to mitigate the impacts of EWEs on urban human mobility. Moreover, this study is of practical significance, especially for policy makers and even city makers, because the findings can provide guidance for urban planning as well as facility layout problems.

DATA AND METHODS

Rainstorm in Nanjing

The city of Nanjing covers a total area of 6,587 km^2 and consists of 94 sub-districts. It has a total population of

8.44 million people. The city experienced a major rainstorm on June 10, 2017, with a total precipitation of over 210 mm. The rainstorm lasted for about one day, and the whole city was severely affected. Based on the precipitation records obtained from Jiangsu Meteorological Bureau, the hourly precipitation in the city during the rainstorm is presented in Table 1. The peak hourly rainfall was over 30mm, which exceeded the threshold of the highest level of rainfall intensity set by the American Meteorological Society (AMS, 2012), setting a new meteorological record of Nanjing in 66 years (Xinhua, 2017).

Table 1. Hourly Precipitation of Nanjing Rainstorm on June 10, 2017

Time	Hourly participation (mm)	Time	Hourly participation (mm)
0:00	0.1	12:00	17.39
1:00	0.2	13:00	24.4
2:00	1.55	14:00	9.83
3:00	4.88	15:00	1.12
4:00	5.07	16:00	3.43
5:00	0.68	17:00	11.66
6:00	5.17	18:00	7.91
7:00	17.75	19:00	2.61
8:00	24.15	20:00	0.38
9:00	22.12	21:00	0.29
10:00	30.68	22:00	0.15
11:00	18.78	23:00	0.1

Data description

Taxi trajectory data

In Nanjing, every taxi reports its vehicle ID, timestamp, longitude, latitude, velocity, angle and passenger status to a central server every 10 seconds during operation through a sensor equipped on it. The data were collected by local authority for transportation management purpose and were not openly available. By working with the local authority, we accessed the trajectory data of all taxis in the city over a period covering the day of the rainstorm (from June 3, 2017 to June 24, 2017). The dataset included about 0.5 billion data entries. The vehicle IDs in the data provided to the us were partially anonymized to protect privacy. The data were cleaned by removing corrupted entries and merging duplicate ones caused by sensor malfunction. A few examples of data entries are shown in Table 2. The number 0 in passenger status means no passenger in the car and 1 means the opposite.

Table 2. Examples of Taxi Trajectory Data Entries

Vehicle ID	Timestamp	Longitude	Latitude	Velocity	Angle	Passenger Status
A9378*	170603004852	118.77095	32.05263	30.89	110	0
A9680*	170603004858	118.80852	32.02560	31.97	92	1
A8866*	170603004847	118.78297	31.99775	0.47	122	1
A9487*	170603004857	118.77473	32.04868	20.77	192	0
A7668*	170603004418	118.71339	32.12084	49.97	52	0
A9764*	170603004850	118.78974	32.04553	8.1	182	0
AB693*	170603004850	118.71868	32.02612	64.98	118	1

POI data

We collected points of interest (POI) data of the entire city from AMap (Open Platform of Amap, 2019), one of the most widely used AutoNavi apps in China, through its online application programming interface (API). The POI dataset consisted of 18,2413 data entries. Each entry had 9 fields, including POI name, POI category, POI type, address, province, city, county, longitude and latitude. There were totally 14 POI categories, which were further divided into 103 POI types. These categories are listed in Table 3, and a few examples of POI data entries are shown in Table 4.

Table 3. A List of POI Categories

Category	
Catering services	Commercial real estate
Scenic spots	Accommodation services
Public facilities	Sports and leisure services
Transportation facilities services	Life services
Enterprises	Medical and health care services
Shopping services	Government agencies and social organizations
Finance and insurance services	Scientific and educational cultural services

Table 4. Examples of POI data entries

POI name	Category	Province	City	County	Longitude	Latitude
** Supermarket	Shopping Service	Jiangsu	Nanjing	Liuhe	118.92477	32.32344
**Plaza	Shopping service	Jiangsu	Nanjing	Liuhe	118.80955	32.52962
**Drugstore	Health care service	Jiangsu	Nanjing	Xuanwu	118.82854	32.10565
**Hospital	Health care service	Jiangsu	Nanjing	Gulou	118.74733	32.06671
**Restaurant	Catering service	Jiangsu	Nanjing	Jiangning	118.86836	31.68686

Methods

Identification of functional area

Drawing on prior research about urban functionalities (Chi et al. 2016, Yuan et al. 2012), the type of function of an urban area belongs to one of the seven categories shown in Table 5. The table also includes a mapping between these categories and the default POI categories in the POI data set.

Table 5. Function Category of POI and Function Types of Urban Area

POI categories in AMap	Type of function of urban areas
Commercial real estate	Real estate
Medical and health care services Scientific and educational cultural services	Education and health care
Catering services Accommodation services Shopping services Finance and insurance services Life services Sports and leisure services	Catering and entertainment
Scenic spots	Parkland
Public facilities Transportation facilities services	Public service facilities

Government agencies and social organizations	Government agencies and social organizations
Enterprises	Enterprises

There were 94 sub-districts in Nanjing, and 93 of them covered an area greater than 1 square kilometer. For fine-grained analysis, we firstly needed to divide the city into square units by certain scale. A smaller unit would likely contribute to the accuracy of the identification of its function type, but would contain fewer trajectory data entries, decreasing the reliability of the calculated mobility perturbation. After comparing the results which were calculated respectively based on 2km × 2km, 1 km × 1km and 500m × 500m grids, we decided to use 1km × 1km grids, which divided the city into around 6400 square units. The distribution of units in terms of the number of POIs within their boundaries is shown in Figure 1.

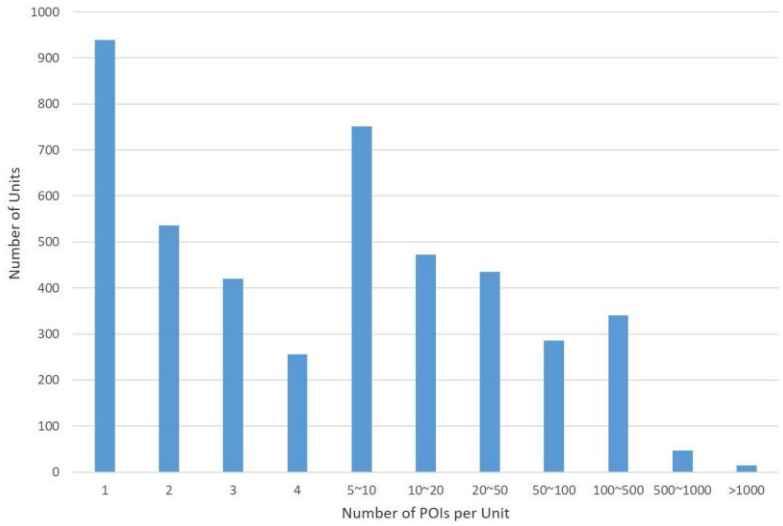

Figure 1. The Number of POIs per Unit

To identify the type of function of each unit, firstly, the numbers of POIs belonging to each of the seven function types were counted for each unit, based on the POI data collected from AMap. Next, we adopted two indicators, namely the frequency density index (F_i) and the ratio index (C_i), which were calculated according to Eq. (7) and Eq. (8) (Chi et al., 2016):

$$F_i = \frac{n_i}{N_i} \ (i = 1,2,3,4,5,6,7) \tag{7}$$

$$C_i = \frac{F_i}{\sum_{i=1}^{7} F_i} \ (i = 1,2,3,4,5,6,7) \tag{8}$$

where N_i is the total number of i-th type of POI, and n_i is the number of i-th type of POI in a unit. Each unity could be represented by a sequence as follows: *[Unit ID, C_1, C_2, C_3, C_4, C_5, C_6, C_7]*. Then, the function type of a unit was determined based on the following principle (Chi et al. 2016):

- When C_i of a unit exceeded 50% for any value of i, this unit was considered to have function type i;
- When C_i of a unit was less than 50% for all values of i, this unit was considered to have a mixed function type;
- When there was no POI within a unit, this unit was considered invalid and hence excluded from the analysis.

After the function type of every unit within the city boundary was identified, the collection of all units with the same function type i was referred to as functional area i hereafter in the paper. In other words, a functional area refers to a collection of units of the same function type distributed across the city. By definition, there were seven types of functional areas.

Assessment of human mobility perturbation

In this study, relative total displacement (*RTD*) is used to measure instantaneous human mobility perturbation of a certain functional area under EWEs based on taxi trajectory data. As a metric measuring human mobility, total displacement (*TD*) is the accumulated consecutive displacements of all taxis in a certain area during a period of

time (Zhang et al., 2019). Based on that definition, total displacement of the x-th unit during the t-th period can be calculated based on Eq. (1):

$$\mathrm{TD_{x,t}} = \sum_{j=1}^{m} \sum_{i=1}^{n-1} d_{ij} \quad (1)$$

where m is the number of taxis traveling in x-th area of the city during t-th timespan, n is the number of locations the j-th taxi visits during this timespan and d_{ij} is the i-th displacement in the trajectory of the j-th individual, which can be calculated based on Eq. (2) (Wang and Taylor 2016):

$$\mathrm{d_{ij}} = 2r \times \sin^{-1}\left(\sqrt{\sin^2\left(\frac{\theta_{i+1,j} - \theta_{i,j}}{2}\right) + \cos\theta_{i+1,j}\cos\theta_{i,j}\sin^2\left(\frac{\varphi_{i+1,j} - \varphi_{i,j}}{2}\right)}\right) \quad (2)$$

where r is the radius of the earth, $\theta_{i,j}$ and $\varphi_{i,j}$ are the latitude and longitude of the former position in the i-displacement of the j-th taxi, and $\theta_{i+1,j}$ and $\varphi_{i+1,j}$ are the latitude and longitude of the latter one.

To calculate the deviation of TD from normal , $\overline{\mathrm{TD}}$, a baseline showing the mobility of taxis in normal time, and RTD can be computed based on Eq. (3) and Eq. (4) (Zhang et al., 2019), where x means the sequence of the unit and t means the sequence of time period:

$$\overline{\mathrm{TD_{x,t}}} = \frac{\sum_{i=1}^{M} TD_{i,x,t}}{M} \quad (3)$$

where these TD values are associated with the same areas, as well as with the same hour of the same day of the week, to avoid daily periodicity, over two weeks before and two weeks after the rainstorm. Then, RTD of the x-th unit during the t-th period can be calculated by normalizing TD with the baseline, $\overline{\mathrm{TD}}$:

$$RTD_{x,t} = \frac{TD_{x,t}}{\overline{TD_{x,t}}} \times 100\% \quad (4)$$

Quantification of accumulated perturbation impacts on human mobility

As an EWE develops over time, its intensity changes, leading to variations in its impacts. These variations, coupled with the fact that urban population tend to adapt to EWE-induced impacts by dynamically adjusting their travel preferences and behaviors (Zanni & Ryley, 2015), may cause human mobility perturbation to be highly fluctuant. It is therefore important to track the fluctuations and evolution of human mobility, and assess the accumulated perturbation impacts throughout the entire timespan of the EWE, for which purpose the metric AP was introduced (Zhang 2019). The AP value of the x-th unit throughout the rainstorm can be calculated based on Eq. (5):

$$AP_x = \int_{t_0}^{t_1} \frac{1 - RTD_{x,t}}{t_1 - t_0} dt \quad (5)$$

where t_0 is the moment of occurrence of perturbation in x-th area, and t_1 is the moment when human mobility totally returns to a normal level.

It needs to be noted that, while in general it is natural to expect human mobility to be impeded by the EWEs, there also exist units where TD might increase in certain short periods of time during the EWEs, especially when the TD is assessed in small spatial scale (e.g. 1 km x 1 km or less). Although decreases and increases in TD are both perturbation to urban mobility, when calculating AP, only decreases in TD are considered, as they indicate negative effect on urban mobility, which is the primary concern when assessing the perturbation to human mobility and resilience of the urban system. Increases of DP in a unit, which may result from temporary increases of operating taxi numbers and varying traffic conditions, indicate that the unit is not experiencing negative impacts during these short periods. If the increases of DP are counted in AP, it would lower the values of AP and hence result in underestimation of the impacts of EWEs. Therefore, when calculating AP, only RTD values between [0,1] were integrated in this study, leading to an adjusted version of Eq. (5):

$$AP_x = \int_{t_0}^{t_1} \frac{1 - RTD_{x,t}}{t_1 - t_0} dt \qquad (when\ RTD_{x,t} < 1) \quad (6)$$

Calculating inflow and outflow

The inflow and outflow of every type of functional area, defined as the number of trips arriving at or leaving the functional area, were calculated in this study. After preprocessing the trajectory data, the information of each trip made by taxi passengers, including its start time, start location, end time and end location, was extracted, as shown in Table 6. When a trip started in a unit, it was counted in the outflow of the functional area that the unit belonged to; Similarly, when a trip ended in a unit, it was counted in the inflow of the functional area that the unit belonged to.

Table 6. Examples of Taxi Ride Record

Start Time	Start Longitude	Start Latitude	End Time	End Longitude	End Latitude
0603061324	118.8838	32.1339	0603061824	118.92477	32.32344
0603065312	118.8827	32.1301	0603071252	118.80955	32.52962
0603075306	118.8869	32.1310	0603084311	118.82854	32.10565
0603093418	118.9446	32.1098	0603093838	118.74733	32.06671

RESULTS

Functional area identification

Based on the method explained in the last section, the function type of each unit within the city boundary was identified, as depicted in Figure 2.

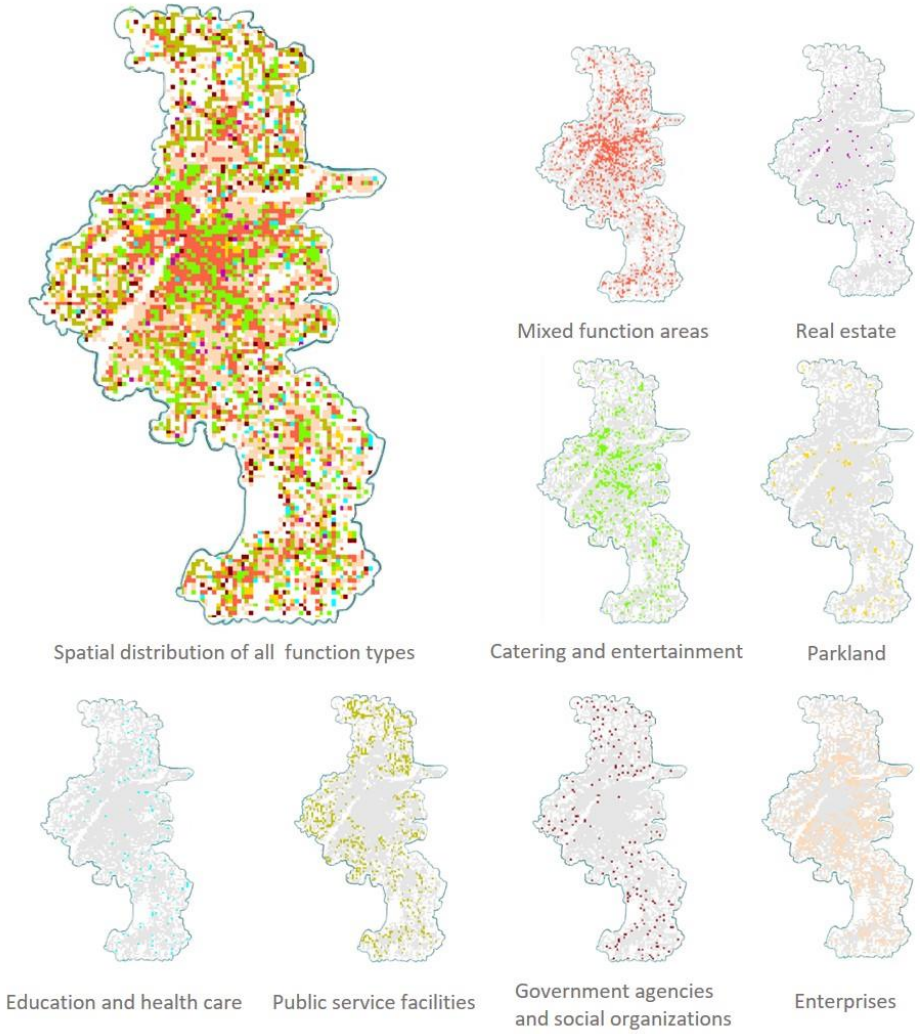

Figure 2. Spatial distribution of Different Functional Areas in Nanjing

In Figure 2, the spatial distributions of eight different functional areas (including mixed functional area) are plotted. Each type of functional area is represented by a different color. The white area within the city boundary indicates invalid units. As summarized in Table 7, there were a total of 4506 valid units. Mixed area and enterprises area accounted for about 56% of all valid units. Real estate area, education and health care area, parkland area and government agencies & social organization area only made up a small proportion of all valid units. In addition, as shown in Figure 2, mixed function area and catering & entertainment area were mainly distributed around city center. Parkland area was mainly located in several regions in the city, and enterprises area showed a trend of aggregation. Education & health care area, public service facilities area and government agency & social organizations area shared a similar spatial distribution. Education & health care area was mainly located in the eastern and southern suburban regions, while the majority of public service facility area was located in western and northern suburban regions.

Table 7. The Number of Different Functional Areas

Functional Area	Number of units	Percentage (%)
Real Estate	55	1.22
Education and Health Care	116	2.57
Catering and Entertainment	716	15.89
Parkland	149	3.31
Public Service Facilities	739	16.40
Government Agencies and Social Organizations	193	4.20
Enterprises	1444	32.05
Mixed Function	1094	24.28
Real Estate	23	2.10
Education and Health Care	40	3.66
Catering and Entertainment	355	32.45
Parkland	20	1.83
Public Service Facilities	104	9.51
Government Agencies and Social Organizations	123	11.24
Enterprises	429	39.21

Mobility perturbation in different functional areas

Selected area

Since each unit only covered an area of one square kilometer and the trajectory data were only collected from taxis, the data entries in some areas were limited for statistical analysis. To ensure the reliability of the results, units with insufficient data points should be excluded. Specifically, if TD value of a unit was 0 in a period of one hour, this period was considered as invalid, and only units with at least 5 valid periods during the entire day of the rainstorm were considered valid units and included in the analysis. The distribution of valid units and their TD values in normal time and during the rainstorm are illustrated in Figure 3, in which blackish color indicates higher TD value and whitish color indicates otherwise. Figure indicates the TD values of the valid units in normal time and during the rainstorm were highly alike, with slight variations in certain regions as highlighted in Figure 3.

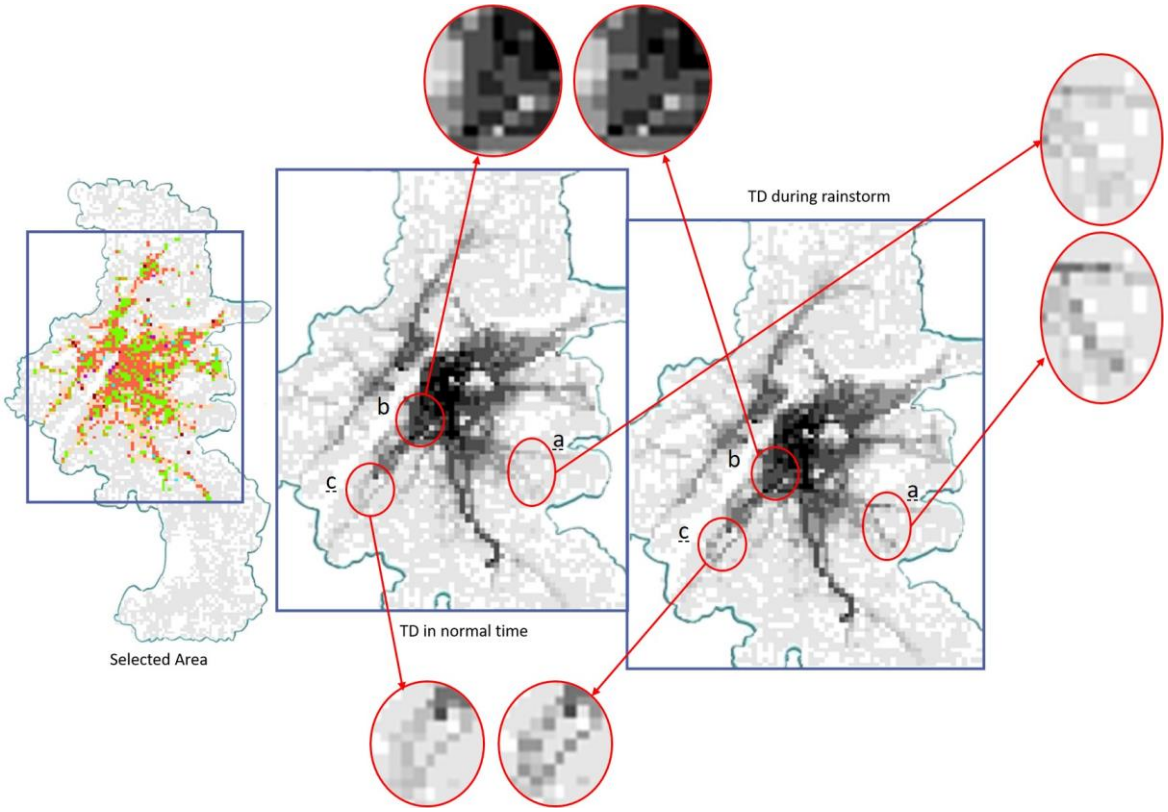

Figure 3. The TD of Units in Normal Time and During Rainstorm

Inflow and outflow in different functional areas

The function of an area has a strong correlation with the traveling behavior of people who visit the area and previous studies adopted inflow and outflow of a certain area to characterize such traveling behavior (Yuan et al., 2012). In this section, the change in inflow and outflow of different functional areas was analyzed to suggest how people's travel behavior was affected under EWEs. The results are illustrated in Figures 4 and 5. The outflow and inflow in catering and entertainment area, enterprises area and mixed function area were higher than other types of functional areas by an order of magnitude, thus they were plotted in two separate subfigures in Figure 4. For all types of functional areas, daily inflow and outflow decreased during the rainstorm, which suggested the rainstorm in general significantly affected the travel demand of the urban population. Among the eight types of functional areas, public service facility area and government & social organizations area were highly affected. The changes in real estate area, parkland area and education & health care area were a little less significant. Catering & entertainment area, enterprises area and mixed function area, with high volumes of inflow and outflow both in normal time and during rainstorm, were only slightly affected.

As can be seen in Figure 5, public services facility area, parkland area and government & social organization area showed biggest variations from normal time, while other areas were relatively alike. This was probably because in the above three types of areas, human activities were sensitive to the impact of EWEs, while human activities in other functional areas were less elastic. Specifically, public service facility area was mainly characterized by POIs such as subway stations, bus stations and other public transportation facilities. The above results indicated that, under the influence of rainstorm, people were less likely to choose public transportation, causing the reduction of travel demand in public service facility related units. According to Figure 5, the impact lasted for an entire day. Similarly, people tended to cancel their trips to parkland or postpone their schedule to government agencies and social organizations during rainstorm, contributing to lower inflow and outflow in these functional areas. The reduction of inflow and outflow in parkland area started from around 9:00 am and lasted until 19:00 pm, while that in government & social organizations area started from 7:00 am and lasted through midnight.

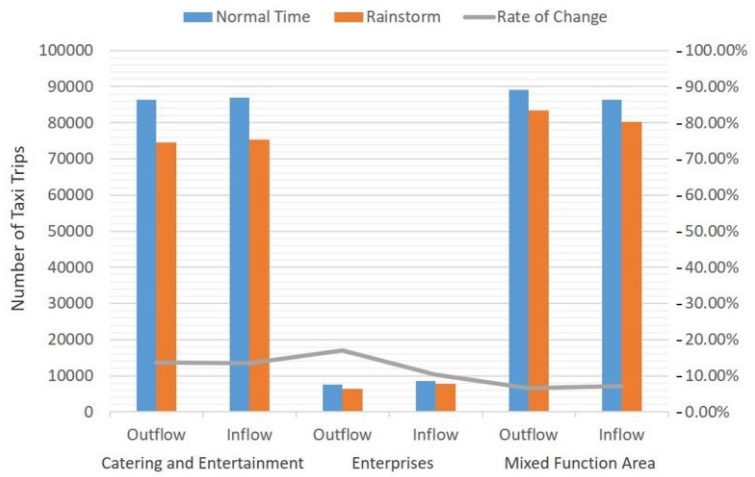

(a)

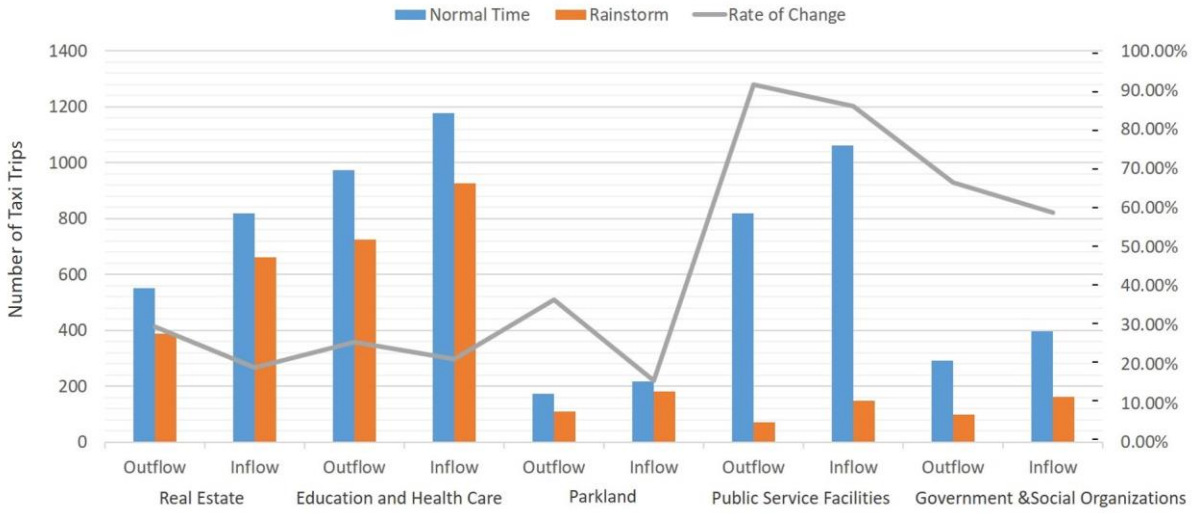

(b)

Figure 4. The Inflow and Outflow of Each Functional Area

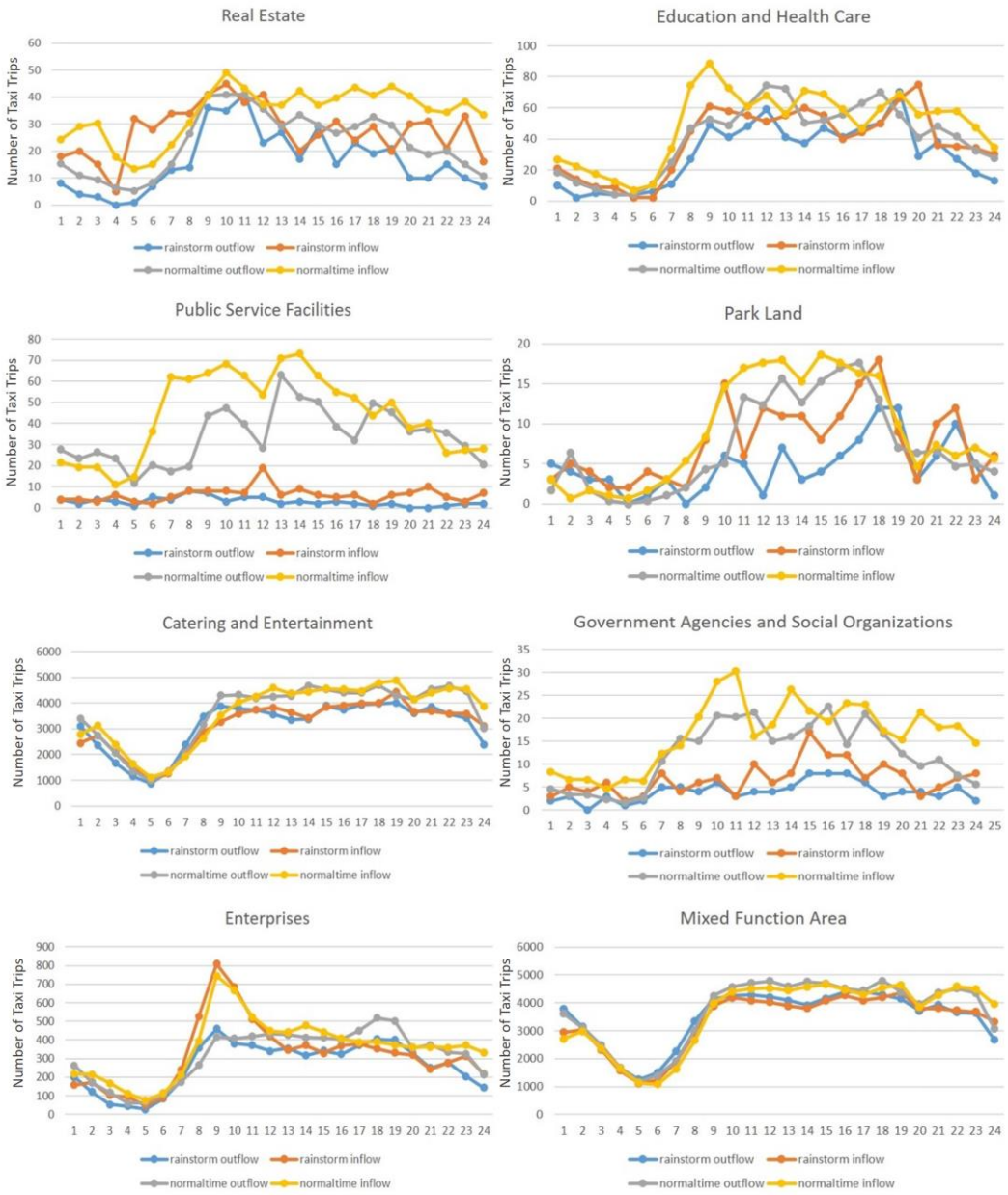

Figure 5. The Inflow and Outflow of Each Function Area throughout the Day

TD in different functional areas

To further analyze and compare the mobility perturbation across different types of functional areas, we calculated TD and AP for each type of functional areas. The moment of occurrence of perturbation and the moment when human mobility totally returns to a normal level were determined using the same approach used in Zhang et al. (2019). The indicator, RTD, assesses the instantaneous perturbation of urban mobility at a given moment, while the indicator AP assesses the accumulated perturbation of urban mobility over the entire lifespan of the EWE. AP, whose value varies between [0,1], indicates the resilience of urban mobility to the impact of EWEs. Smaller AP values indicates higher levels of resilience. According to Table 9, enterprises areas were the most resilient among all eight types of functional areas, and parkland areas were the least resilient. Maybe it's because that the rainstorm happened on Saturday when people normally spend their time in parkland areas. Influenced by rainstorm, the operating taxis in parkland areas decreased seriously, contributing to higher AP. However, for enterprises area, human mobility is mostly contributed from commuting behaviors, which are relatively more stable and less influenced by rainstorm. Therefore, enterprises areas showed high resilience during rainstorm. It can be also informed that though real estate areas and education & health care areas experienced similar changes in inflow and outflow, TD of these two types of areas were influenced differently. More specifically, TD in real estate areas decreased during rainstorm, whereas TD in education and health care areas increased. Furthermore, education and

health care areas were more resilient than real estate areas. It was also found that, even though highly influenced in terms of travel demand, public service facility areas were relatively resilient. In addition, the spatial variance of AP is illustrated in Figure 6. It is shown that units located in different regions, even if belonging to the same function area, may have significantly different AP values. This suggested that the AP value of a unit was to some extent determined by its spatial characteristic.

Table 9. TD and AP of Each Functional Area

Area	TD during rainstorm (km)	TD in normal time (km)	AP
0.Real Estate	5506310.50	6002198.00	0.1585
1.Education and Health Care	2203730.30	2173677.60	0.1170
2.Catering and Entertainment	212458820.00	242035220.00	0.1278
3.Parkland	779604.46	1344520.40	0.4140
4.Public Service Facilities	2228126.60	2068161.10	0.1368
5.Government and Social Organizations	828194.60	769447.50	0.1531
6.Enterprises	50175947.00	51352692.00	0.1031
7.Mixed Function Area	309718640.00	360035670.00	0.1293

When comparing the temporal variance of TD in normal time and during rainstorm (see Figure 7), it was found that different functional areas showed different degrees of resilience. While several functional areas experienced an obvious decrease in TD, other functional areas saw increases in TD in certain short periods during the rainstorm. For catering & entertainment areas and mixed function areas, TD began to be affected from 7:00 am, and then the impact gradually expanded. Parkland areas were the most affected, and the impact lasted from 7:00 am to 9:00 pm, which suggested human mobility in these areas was more sensitive to the influence of rainstorm than others.

Figure 6. The Spatial Variance of AP in Different Functional Areas

Figure 7. TD and RTD Curve for Each Functional Area

Distance to city center and mobility perturbation

As Figure 6 suggests, units of the same functional area may have significantly different AP values, at least partly depending on where in the city they were located. One major factor that determined the spatial characteristic of a unit was its distance to the city center. Hence, it was hypothesized that a unit's distance to city center may determine its magnitude of mobility perturbation. To test this hypothesis, we depicted Figure 8, in which blackish color indicates smaller AP values and hence higher resilience, and whitish color indicates the opposite. It can be seen in the figure that the AP values of units near the city center were notably larger, while those located in suburban areas were smaller. The relationship between a unit's distance to city center and its RTD and AP values is further shown in Figure 9. This results suggested that, for all types of functional areas, units that were distant from the city center were relatively less influenced by the rainstorm.

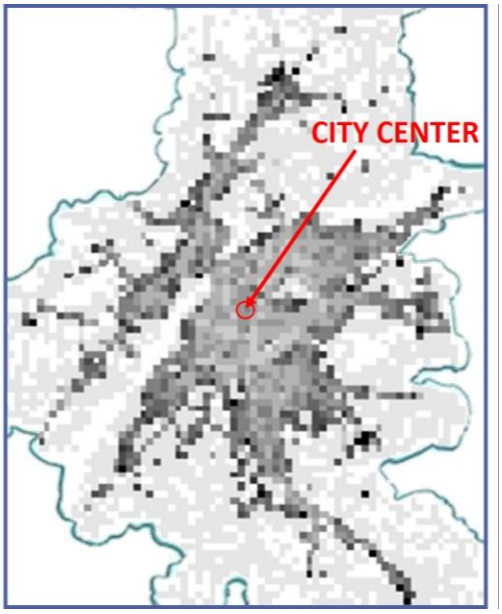

Figure 8. The Distribution of AP in Selected Area

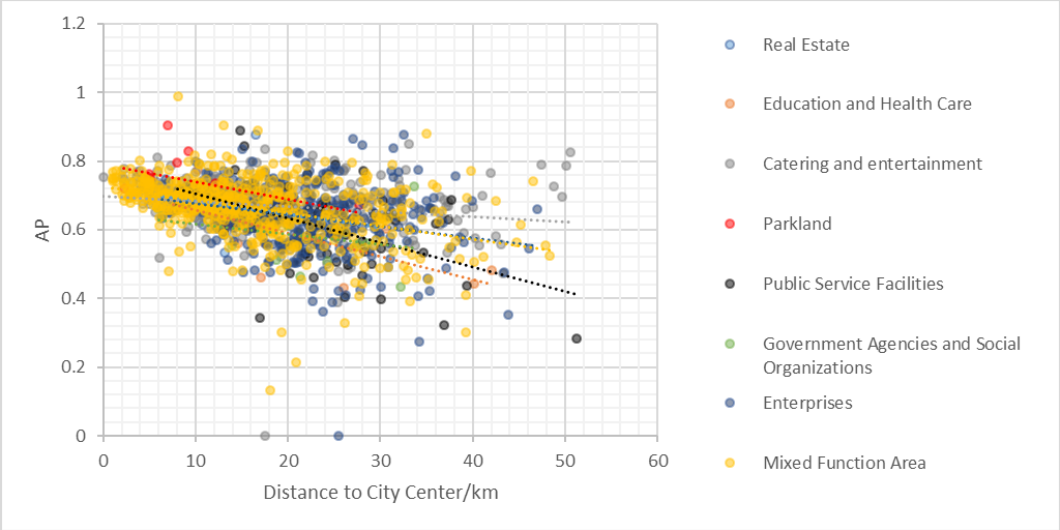

Figure 9. Correlation between Distance to City Center and AP Values

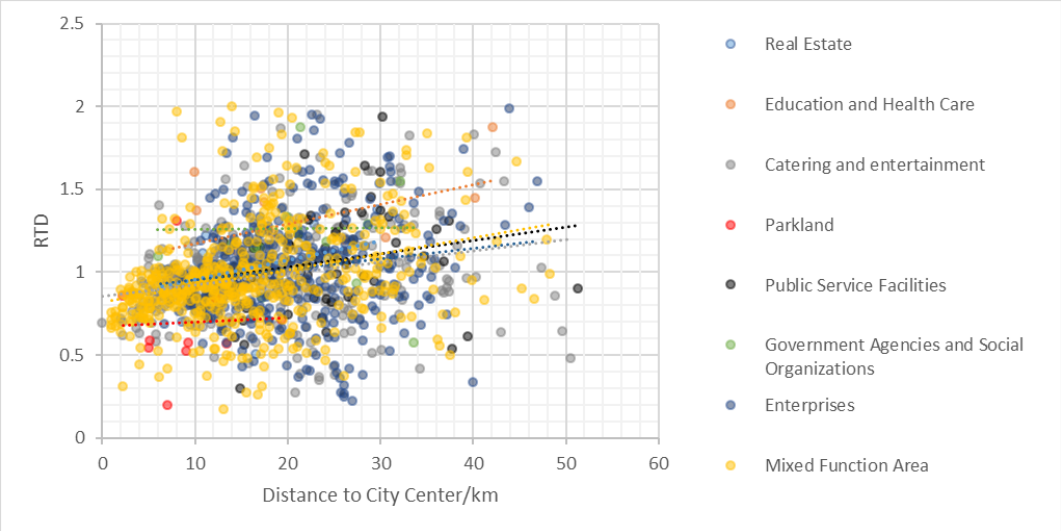

Figure 10. Correlation between Distance to City Center and RTD Values

CONCLUSIONS

This study aimed to explore the correlation between EWE-induced human mobility perturbation in urban areas and their spatial characteristics, by examining a case study of a major rainstorm in the City of Nanjing in 2017. We divided Nanjing into small units, and extracted the spatial characteristic of these units, including their function type and distance to city center. Based on taxi trajectory data before, during and after the rainstorm, we assessed the spatial and temporal characteristics of human mobility perturbation in each unit, and correlated the assessment results with the spatial characteristics of the units. The findings showed that travel demand decreased in all types of functional areas during rainstorm. It was also found that human mobility in different types of functional areas were influenced by the EWEs to different degrees, showing different levels of resilience. In addition, areas far from the city center were generally less influenced by the rainstorm. These findings are expected to contribute to the understanding of the variance of mobility perturbation among different areas in a city, which would allow a more fine-grained prediction of influence caused by EWEs, hence supporting the mitigation of EWE-induced impacts and strengthening the urban crisis management practices.

That being said, there are several limitations in this study that are noteworthy. Firstly, urban areas may have certain spatial characteristics that are not fully reflected by their POIs, therefore complementary data may be needed to better represent their spatial characteristics. Secondly, the human mobility and its perturbation was assessed based on taxi trajectories, which could not reflect the mobility associated with other modes of transport, and due to the nature of the trajectory data, the analysis could not be done at the individual passenger level. This issue could be resolved once other types of human mobility data such as mobile phone trajectories are made

available. More importantly, this study mainly focused on unrevealing the statistical relationships between urban areas' spatial characteristics and their EWE-induced mobility perturbation, however, the underlying mechanisms that shape such relationships still require further investigation in future research.

ACKNOWLEDGMENTS

This work was supported by the National Natural Science Foundation of China (NSFC) under grant No. 71974105. The authors are grateful for the support of NSFC. Any opinions, findings, and conclusions or recommendations expressed in this paper are those of the authors and do not necessarily reflect the views of the funding agency.

REFERENCES

Belik, V., Geisel, T., & Brockmann, D. (2011). Natural Human Mobility Patterns and Spatial Spread of Infectious Diseases. Physical Review X, 1(1), 1–5. https://doi.org/10.1103/PhysRevX.1.011001

Bordoloi, R., Mote, A., Sarkar, P. P., & Mallikarjuna, C. (2013). Quantification of land use diversity in the context of mixed land use. Procedia-Social and Behavioral Sciences, 104, 563-572.

Chi, J., Jiao, L., Dong, T., Gu, Y., & Ma, Y. (2016). Quantitative identification and visualization of urban functional area based on poi data. *Journal of Geomatics*, 41(2), 68-73.

Collins, A. (2018). The global risks report 2018. In Geneva: World Economic Forum.

Ding, C., Cao, X., & Liu, C. (2019). How does the station-area built environment influence Metrorail ridership? Using gradient boosting decision trees to identify non-linear thresholds. Journal of Transport Geography, 77, 70-78.

Fang, D., Li, Z., Han, L., Wu, J., & Lu, X., et al. (2017) Urban resilience: a perspective of system of systems in trio spaces. *China Civil Engineering Journal, 50*(7), 1-7.

Force, H. S. R. T. (2013). Hurricane Sandy Rebuilding Strategy, US Department of Housing and Urban Development.

Forzieri, G., Feyen, L., Russo, S., Vousdoukas, M., Alfieri, L., Outten, S., ... & Cid, A. (2016). Multi-hazard assessment in Europe under climate change. Climatic Change, 137(1-2), 105-119.

Godschalk, D. R. (2003). Urban hazard mitigation: creating resilient cities. Natural hazards review, 4(3), 136-143.

Horner, M. W., & O'Kelly, M. E. (2001). Embedding economies of scale concepts for hub network design. Journal of Transport Geography, 9(4), 255–265. https://doi.org/10.1016/S0966-6923(01)00019-9

IPCC (2014). Annex II: Glossary [Mach, K.J., S. Planton and C. von Stechow (eds.)]. In: Climate Change 2014: Synthesis Report. Contribution of Working Groups I, II and III to the Fifth Assessment Report 537 of the Intergovernmental Panel on Climate Change. IPCC, Geneva, Switzerland, pp 117-130

Jeff Berardelli. (2018). 2018's top 3 most expensive climate-driven events took place in U.S.. CBS NEWS. https://www.cbsnews.com/news/extreme-weather-events-2018-top-3-most-expensive-climate-driven-events-took-place-in-us/. Accessed in 29 December 2018.

Krings, G., Calabrese, F., Ratti, C., & Blondel, V. D. (2009). Urban gravity: A model for inter-city telecommunication flows. Journal of Statistical Mechanics: Theory and Experiment, 2009(7), 1–8. https://doi.org/10.1088/1742-5468/2009/07/L07003

Leichenko, R. (2011). Climate change and urban resilience. Current opinion in environmental sustainability, 3(3), 164-168.

Liang, X., Zhao, J., Dong, L., & Xu, K. (2013). Unraveling the origin of exponential law in intra-urban human mobility. Scientific reports, 3, 2983.

Lu, X., Wrathall, D. J., Sundsøy, P. R., Nadiruzzaman, M., Wetter, E., Iqbal, A., ... & Bengtsson, L. (2016). Unveiling hidden migration and mobility patterns in climate stressed regions: A longitudinal study of six million anonymous mobile phone users in Bangladesh. Global Environmental Change, 38, 1-7.

Noulas, A., Scellato, S., Lambiotte, R., Pontil, M., & Mascolo, C. (2012). A tale of many cities: universal patterns in human urban mobility. PloS one, 7(5), e37027.

Open Platform of Amap. (2019). Retrieved July 3, 2019, from: https://lbs.amap.com

Sobel, A. H., & Tippett, M. K. (2018). Extreme events: trends and risk assessment methodologies. In Resilience (pp. 3-12). Elsevier.

Stott, P. (2016). How climate change affects extreme weather events. Science, 352(6293), 1517-1518.

Stouffer, S. A. (1940). Intervening opportunities: a theory relating mobility and distance. American sociological review, 5(6), 845-867.

Van Aalst MK (2006) The impacts of climate change on the risk of natural disasters. Disasters 30: 5-18.

Wang, Q. (2014). Quantifying, Comparing Human Mobility Perturbation during Hurricane Sandy, Typhoon Wipha, Typhoon Haiyan. Procedia Economics and Finance, 18, 33-38.

Wang, Q., & Taylor, J. E. (2014). Quantifying human mobility perturbation and resilience in Hurricane Sandy. PLoS one, 9(11), e112608.

Wang, Q., & Taylor, J. E. (2016). Patterns and limitations of urban human mobility resilience under the influence of multiple types of natural disaster. *PLoS one, 11*(1), e0147299.

Wang, Y., Wang, Q., & Taylor, J. E. (2017). Aggregated responses of human mobility to severe winter storms: An empirical study. PloS one, 12(12), e0188734.

Yabe, T., Tsubouchi, K., Sudo, A., & Sekimoto, Y. (2016, October). A framework for evacuation hotspot detection after large scale disasters using location data from smartphones: case study of kumamoto earthquake. In Proceedings of the 24th ACM SIGSPATIAL International Conference on Advances in Geographic Information Systems (p. 44). ACM.

Yang, Y., He, Z., Song, Z., Fu, X., & Wang, J. (2018). Investigation on structural and spatial characteristics of taxi trip trajectory network in Xi'an, China. Physica A: Statistical Mechanics and its Applications, 506, 755-766.

Yuan, J., Zheng, Y., & Xie, X. (2012, August). Discovering regions of different functions in a city using human mobility and POIs. In Proceedings of the 18th ACM SIGKDD international conference on Knowledge discovery and data mining (pp. 186-194). ACM.

Zanni, A. M., & Ryley, T. J. (2015). The impact of extreme weather conditions on long distance travel behavior. Transportation Research Part A: Policy and Practice, 77, 305–319.

Zhang, F., Li, Z., Li, N., & Fang, D. (2019). Assessment of Urban Human Mobility Perturbation under Extreme Weather Events: A Case Study in Nanjing, China. *Sustainable Cities and Society*, 101671.

Zheng, Z., & Zhou, S. (2017). Scaling laws of spatial visitation frequency: Applications for trip frequency prediction. Computers, Environment and Urban Systems, 64, 332-343.